FM Mode-Locked Fiber Lasers Operating in the Autosoliton Regime

Nicholas G. Usechak, Govind P. Agrawal, *Fellow, IEEE*, and Jonathan D. Zuegel

***Abstract*—A high-repetition-rate ytterbium fiber laser, harmonically mode-locked using a phase modulator, is investigated experimentally, numerically, and analytically. Experimental results agree well with numerical simulations using the measured parameter values. By employing a few approximations, our model is cast in terms of a Ginzberg–Landau equation. This equation has known analytic solutions that agree well with the results of the full model in the appropriate limit. Pulse stability is also investigated numerically with an emphasis on the role of third-order dispersion.**

***Index Terms*—Autosolitons, fiber lasers, FM mode-locked lasers.**

I. Introduction

IT IS WELL known that the propagation of ultrashort pulses in optical fiber is governed by the nonlinear Schrödinger equation (NLSE) [1]. In the anomalous-dispersion regime, this equation allows for the fundamental-soliton solution that represents an optical pulse whose shape and width are invariant under propagation. In the context of fiber lasers, the NLSE must be modified to account for loss, gain, gain filtering, and a mode-locking element. Although the resulting equation has no closed form solution, passive mode-locking mechanisms, such as nonlinear polarization rotation, nonlinear fiber-loop mirror, and saturable absorption, produce "soliton-like" pulses [2].

Contemporary investigations into actively mode-locked lasers in the presence of dispersion and nonlinearity have not attracted as much attention as the above-mentioned passive techniques. This is most likely due to the shorter pulse durations that the passive approaches produce. Of course, there is still a demand for actively mode-locking lasers since doing so provides a simple means by which one can ensure self-starting, increase the laser's repetition rate (through harmonic mode locking), and synchronize the laser pulses to a master clock [3], [4]. In a laser devoid of dispersion and nonlinearity, both amplitude modulation (AM) and frequency modulation (FM) mode-locking techniques produce Gaussian pulses [5]. However, the existence of an FM mode-locked "soliton" laser in the presence of these effects has not yet been fully investigated.

Manuscript received November 21, 2004; revised January 28, 2005. This work was supported by the U.S. Department of Energy Office of Inertial Confinement Fusion under Cooperative Agreement DE-FC03-92SF19460, in part by the University of Rochester, and in part by the New York State Energy Research and Development Authority. The support of DOE does not constitute an endorsement by DOE of the views expressed in this article.

N. Usechak and G. Agrawal are with the Institute of Optics, University of Rochester, Rochester, NY 14627 USA. They are also with the Laboratory for Laser Energetics, University of Rochester, Rochester, NY 14623 USA (e-mail: noodles@optics.rochester.edu; gpa@optics.rochester.edu).

J. Zuegel is with the Laboratory for Laser Energetics, University of Rochester, Rochester, NY 14623 USA (e-mail: zuegel@lle.rochester.edu).

Digital Object Identifier 10.1109/JQE.2005.846695

Haus and Silberberg were the first to address the effects of dispersion and nonlinearity on actively mode-locked lasers in 1986 [6]. They found that the pulsewidth in an AM mode-locked laser can be reduced inside the cavity by introducing a nonlinear medium. This effect, known as soliton pulse compression, was first experimentally demonstrated in an actively mode-locked fiber laser by Kafka *et al.* in 1989 [7]. Later, Kärtner *et al.* applied soliton perturbation theory to show that a stable soliton can exist in an AM mode-locked laser which incorporates dispersive and nonlinear elements [8]. Other relevant work numerically compared both AM and FM mode-locked lasers to show that, in the presence of a Kerr medium, both pulse profiles become increasingly "sech-like" as either the gain is increased [9] or the modulation depth is decreased (AM only) [10]. More recent efforts have addressed soliton stability in AM mode-locked, inhomogeneously broadened, lasers [11].

Given the body of literature addressing actively mode-locked lasers, it is surprising to note that no concentrated effort has been directed toward FM mode-locked "soliton" lasers. Since such a venture may seem to be a logical extension of the prior AM efforts we point out that AM- and FM-mode-locking schemes differ in key areas. FM mode-lockers interact with self-phase modulation (SPM) in a direct manner, whereas AM mode-lockers affect the cavity loss and literally carve pulses out of CW light. As a consequence, FM mode lockers do not require biasing while their AM counterparts do [12]. Although it is well known that FM mode-locked lasers can jump between two degenerate operating states [13], a dispersive laser cavity breaks this degeneracy and suppresses the laser's tendency to switch states [12], [14]. Experimental work with FM mode-locked fiber lasers has also produced quasi-transform-limited pulses with time-bandwidth-products as low as 0.30 [15], indicating "soliton" formation [12], [15]–[17]. Still, the lack of an analytic theory capable of explaining FM mode-locking in fiber lasers is not surprising in view of the difficulty in solving the governing nonlinear equation with the inclusion of an active mode-locking element.

In this work, we investigate the operation of a high-repetition-rate, harmonically FM mode-locked, ytterbium fiber laser experimentally [18], numerically, and analytically. In Section II we describe the laser and present our experimental data. The approach used to model the laser is discussed in Section III where the numerically obtained results agree well with the experimental data. The issue of pulse stability is addressed in Section IV and the role of third-order dispersion (TOD) on pulse switching is noted. Section V shows that averaging the parameters, used in the model developed in Section III, over the cavity length results in a modified Ginzburg–Landau equation.

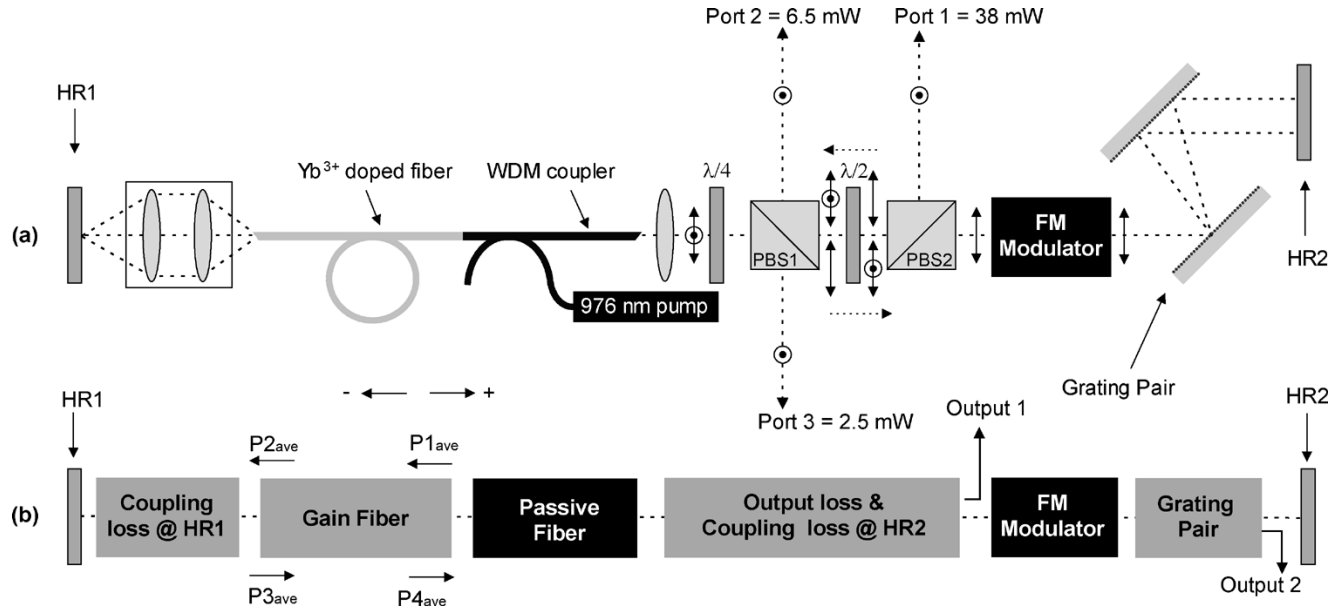

Fig. 1. (a) Experimental laser configuration: HR, high-reflectivity mirrors; PBS, polarizing beam splitters; WDM, wavelength division multiplexer. The double sided arrows and the dots surrounded by circles represent the horizontal and vertical polarizations respectfully. (b) Numerically modeled laser configuration: the coupling losses take into account all cavity losses at the respective cavity ends, including the laser outputs.

This equation is then used to argue that the mode-locked pulses can be approximately treated as autosolitons. The results of this approach are found to be in good agreement with the numerical simulations when intracavity losses are reduced.

II. Experimental Results

The FM technique has been used to mode-lock erbium fiber lasers with time-bandwidth products as low as 0.30 [15]. Although it has been suspected that this type of laser can produce hyperbolic-secant pulses [9], [12], [14], [15], neither the shape of the output pulses nor their spectra were experimentally investigated further than the fitting of autocorrelation traces. Most ytterbium fiber lasers reported to-date have used a passive mode-locking mechanism to take advantage of ytterbium's broad gain bandwidth and generate short pulses at relatively low repetition rates ($\leq$ 100 MHz). For example, a ytterbium fiber laser produced 36 fs mode-locked pulses [19], the shortest to-date from any fiber laser, however, the repetition rate was below 50 MHz.

Ytterbium's large saturation fluence has also been exploited in the pursuit of high-power amplifiers and lasers. This feature also makes it an ideal gain medium for mode-locking at higher harmonics where the laser's power must be split among a large number of circulating pulses. Recently, we used the FM technique in a ytterbium fiber laser to produce mode-locked pulses at a high repetition rate exceeding 10 GHz [18]. The laser configuration is shown in Fig. 1(a) where the combination of a half-wave plate ($\lambda/2$) and polarizing beam splitter (PBS2) not only provides variable output coupling, but also sets a linear polarization for the FM modulator and the grating pair. The measured average power at each of the three output ports is also indicated in Fig. 1(a).

A 30-mW mode-locking threshold was measured, but the 976-nm pump laser was operated at 150 mW to maximize the output power. All of the experimental results were obtained at this pump power using the output from port 1. The cavity also incorporates a grating pair to compensate the normal dispersion introduced by 1 m of ytterbium-doped fiber and 1.2 m of fiber associated with the 976/1050-nm wavelength division multiplexing (WDM) coupler. The net second- and third-order cavity dispersions, $d_2 = \int_0^L \beta_2(z)dz$ and $d_3 = \int_0^L \beta_3(z)dz$ (where L is the distance during one round-trip within the cavity and β_2 and β_3 are the second- and TOD parameters), were measured to be $d_2 = -6.3 \times 10^4$ fs^2 and $d_3 = 130.6 \times 10^4$ fs^3, respectively. This measurement, performed using an *in situ* technique [20], shows that this laser operates in the anomalous-dispersion regime.

All intracavity losses at the grating-pair side of the cavity (including the laser outputs) were measured individually and combined for a total power loss of 96% as the pulses pass through the grating pair, FM modulator, and the PBSs. Power losses at the HR1 cavity end were estimated to be approximately 20%. The small signal gain of the ytterbium-doped fiber was measured to be 4.3 ± 0.4 m^{-1} by using a narrow-band CW laser (Koheras Y10-PM) operating at 1053 nm. The gain-bandwidth was approximated by the 25-nm full-width at half-maximum (FWHM) of the amplified spontaneous emission (ASE) spectrum.

The optical spectrum of the mode-locked pulses is shown in Fig. 2 and has a FWHM of 0.8 nm. This spectrum is best fit by a function of the form $S(w) = S_0 \mathrm{sech}^2[(w - w_0)/\Delta w]$, as shown by the dotted curve in Fig. 2 (almost indistinguishable from the numerically obtained result which is discussed in Section III) where $\Delta w/2\pi = 746$ GHz. For comparison, the dashed curve shows the poor agreement obtained when a Gaussian fit is used. Assuming a transform-limited $\mathrm{sech}^2(t/\Delta t)$ pulse shape, this corresponds to a temporal pulsewidth of $\Delta t = 0.85$ ps (FWHM $= 1.5$ ps). Interferometric autocorrelation measurements, performed using two-photon absorption inside a photomultiplier tube [21], yield a temporal FWHM of 2.0 ± 0.5 ps. This measurement indicates that our pulses are close to their transform limit.

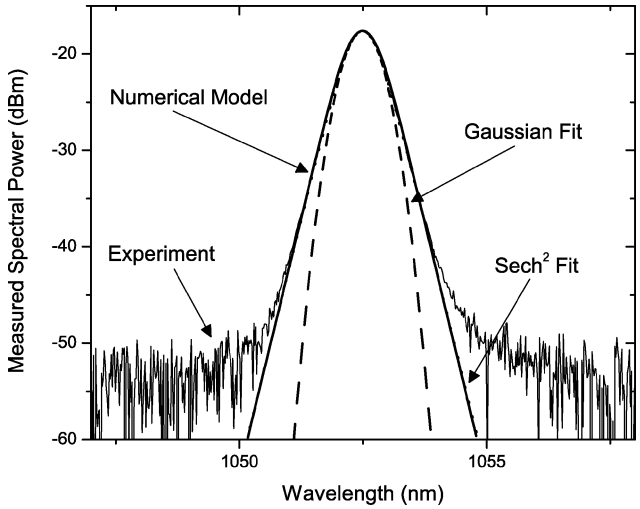

Fig. 2. Experimentally measured pulse spectrum (solid curve with − 55 dBm noise background), a hyperbolic secant fit (dotted), a Gaussian fit (dashed), and the numerically simulated spectrum (solid).

In our actively mode-locked fiber laser the characteristic dispersion and nonlinear lengths are much longer than the 2.2 m of fiber in the cavity. The dispersion length, $L_D = T_0^2/|\beta_2|$, for the 2-ps pulses is 45 m using the fiber's dispersion parameter $\beta_2 = 2.81 \times 10^4$ fs^2/m, or 90 m when using the cavity's average dispersion of $\bar{\beta}_2 = -1.43 \times 10^4$ fs^2/m. The nonlinear length $L_{NL} = (\gamma P_0)^{-1} = 73.5$ m is calculated using a 1.13-W peak power (derived using an estimated average power of 26.5 mW in the fiber and 2-ps hyperbolic secant pulses) and the nonlinear parameter $\gamma \approx 0.012$ W^{-1}/m (mode field diameter≈ 4.1 μm, $n_2 = 2.6 \times 10^{-20}$ m^2/W). Nonlinear polarization rotation of the intracavity field inside the 2.2 meters of fiber is negligible during a single round-trip; moreover the polarizing beam splitter, PBS1, does not allow this effect to accumulate over multiple round-trips. This viewpoint was experimentally confirmed by noting that rotating the quarter waveplate ($\lambda/4$) does not significantly affect the mode-locking ability of the laser, although it does affect the spectral bandwidth due to the amount of loss introduced by PBS1. As a result, the pulse is not strongly affected by the dispersive and nonlinear effects during a single round-trip, although these effects are certainly important over multiple round-trips. We stress that this is in sharp contrast with passively mode-locked fiber lasers where polarization can change considerably during a single round-trip due to nonlinear effects. Moreover, in passively mode-locked fiber lasers the nonlinear and dispersion lengths can be comparable with the cavity length.

III. Numerical Simulations

A vector NLSE is generally required to describe pulse propagation in fiber lasers [1], however, we have already shown that nonlinear polarization rotation in our fiber laser is negligible. Assuming dynamic polarization effects can be neglected, the vector equation can be reduced to the following scalar equation

$$\frac{\partial A}{\partial z} + i\frac{\beta_2}{2}\frac{\partial^2 A}{\partial t^2} - \frac{\beta_3}{6}\frac{\partial^3 A}{\partial t^3} = i\gamma |A|^2 A - \frac{1}{2}\alpha A + \frac{1}{2}\int_{-\infty}^{\infty} g(t-t',z)A(t',z)dt' \quad (1)$$

where

$$g(t,z) = \frac{g_0(z)}{1 + \frac{P_{\rm ave}(z)}{P_{\rm sat}}} \int_{-\infty}^{\infty} \tilde{g_s}(\omega) e^{-i\omega t} d\omega. \quad (2)$$

In this equation, A represents the slowly varying envelope of the optical field, β_2 and β_3 account for the second- and third-order fiber dispersion, and γ is the nonlinear parameter of the fiber. The fiber loss is given by α and the gain, whose time dependence results from a finite gain bandwidth, is given by $g(t,z)$. Since the gain bandwidth of our ytterbium fiber was estimated to be 25 nm ($\Delta w_g/2\pi = 6.759$ THz) and the laser produced pulses with less than 1 nm of bandwidth, the spectral filtering is not expected to strongly influence the pulse shape and the gain spectrum is approximated by a parabola $\tilde{g_s}(\omega) = (1 - 4\,\omega^2/\Delta\omega_g^2)$. We also assumed that the small signal gain over the 1 m of doped fiber is approximately constant, setting $g_0(z) = g_0$. Since the temporal separation between adjacent pulses in this laser ($\sim$ 100 ps) is much shorter than the relaxation time of ytterbium ($\sim$ 1.5 ms), the gain is saturated by the location-dependent average power of the pulses as shown in (2). The location dependent average power was determined using

$$P_{\rm ave}^{\pm}(z) = \frac{1}{T_m}\int_{-T_m/2}^{T_m/2} \left|A^{\pm}(t,z)\right|^2 dt \quad (3)$$

where $T_m = F_{\rm rep}^{-1}$ is the duration of a single modulation cycle and $F_{\rm rep}$ is the frequency with which our modulator is driven. The $+$ and $-$ superscripts denote the direction in which the field propagates as defined in Fig. 1(b). In (2) $P_{\rm ave}(z)$ was computed by summing the average powers of the counter propagating pulses for each spatial step using $P_{\rm ave}(z) = P_{\rm ave}^{+}(z) + P_{\rm ave}^{-}(z)$. The gain saturation power, $P_{\rm sat} = 24$ mW, was estimated by requiring that the model produce the measured average output power of $P4_{\rm ave} = 62$ mW [see Fig. 1(b)].

Our model uses (1) to propagate the pulses within the laser's active $[g_0(z) = g_0]$ and passive $[g_0(z) = 0]$ fiber sections. It then considers the influence of the other cavity elements individually, as depicted in Fig. 1(b). For example, we assume that the 600-grooves/mm grating pair acts as a dispersive element introducing single-pass second-order dispersion ($d_2^g = -9.34 \times 10^4$ fs^2) and TOD ($d_3^g = 17.0 \times 10^4$ fs^3) into the cavity based on its configuration (30° incident angle, 12-cm separation) [22]. The losses associated with the grating pair were lumped into a combined loss at the end mirror HR2, as previously noted in Section II.

The FM modulator was treated as if it modified an incident field $A_{\rm in}$ according to [5]

$$A_{\rm out}(t) = e^{i\Delta\cos(\omega_m t + \phi)} A_{\rm in}(t) \quad (4)$$

where $\omega_m = 2\pi F_{\rm rep}$ is the modulation frequency, assumed throughout this work to be a harmonic of the laser's fundamental repetition rate. Any time delay between the modulator and the pulse reference frame is accounted for by ϕ in (4), which was set to zero unless otherwise noted. Using a high-resolution optical spectrum analyzer and a continuous-wave semiconductor laser (Sacher Lasertechnik TEC 500) operating at 1.05 μm, the modulation depth, $\Delta = 0.45$, was measured when driving the modulator with the same frequency (10.3 GHz) and power (10 W)

TABLE I
PARAMETER VALUES USED IN NUMERICAL SIMULATIONS

$\beta_2 = 2.81 \times 10^4$ fs^2/m	$\beta_3 = 22 \times 10^4$ fs^3/m	$\alpha = 0.0$ m^{-1}	$\gamma = 0.012$ W^{-1}/m
$d_2^g = -9.34 \times 10^4$ fs^2	$d_3^g = 17.0 \times 10^4$ fs^3	HR1 Power Loss $= 20$ %	HR2 Power Loss $= 96$ %
$g_0 = 4.3$ m^{-1}	$\Delta w_g = 42.54 \times 10^{12}$ rad/sec	$P_{sat} = 24$ mW	$\lambda_0 = 1052.53$ nm
$F_{rep} = 10.3$ GHz	$\Delta = 0.45$	$\phi = 0$ rad	$L_{gain} = 1.0$ m
$L_{WDM} = 1.2$ m			

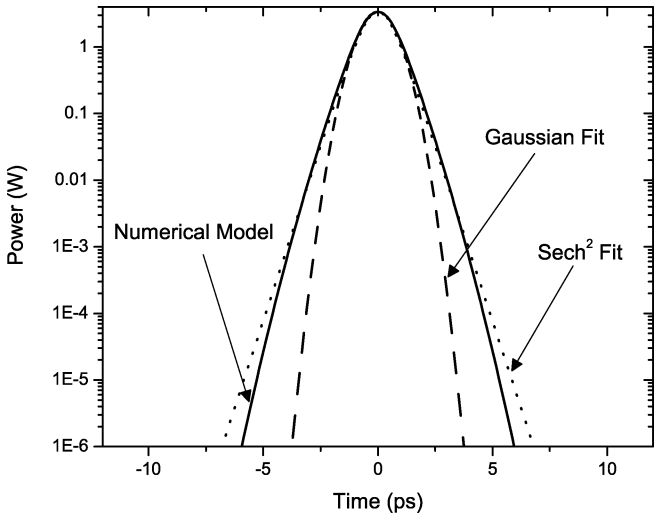

Fig. 3. Numerically predicted temporal profile of mode-locked pulses (solid), hyperbolic secant fit (dotted), and a Gaussian fit (dashed).

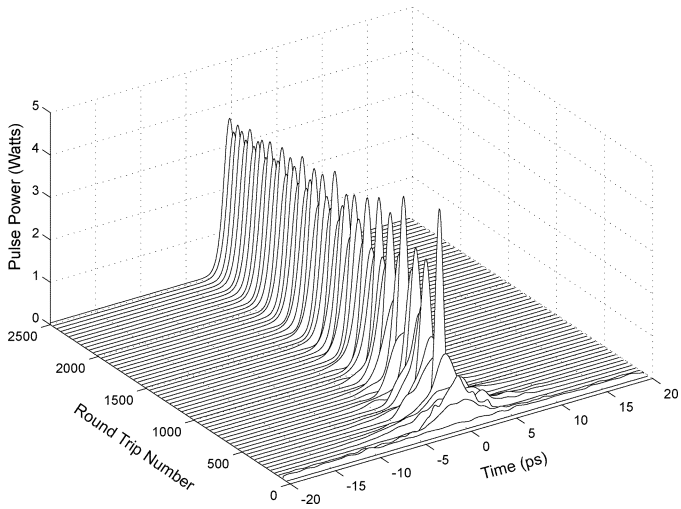

Fig. 4. Numerically simulated pulse formation from noise. Note that the laser has not converged to a steady state even after 2500 round-trips.

used to mode-lock the laser. All of the parameter values used in our simulations are summarized in Table I for convenience.

The model considers a laser mode-locked at its 281st harmonic by using a 97-ps temporal simulation window together with periodic boundary conditions. This simplification is commonly used and justified, in this case, through the experimental observation of low pulse-pulse amplitude and timing jitter. Furthermore, a side-mode suppression measured to be > 70 dB indicates that neighboring pulses exhibit a high degree of similarity [18].

Fig. 1(b) shows the block diagram used to model the laser shown in Fig. 1(a). The model "unfolds" the laser cavity, passing the slowly varying field, A, through each cavity component twice during a single round-trip. The numerical results, taken at "output 1" [specified in Fig. 1(b)] and shown by the solid curve in Fig. 2 (the experimental results were also extracted from the same location), were obtained by solving this problem using the symmetric split-step method [1] on a 1024-point temporal grid with 200 spatial steps per round-trip. The simulated spectrum matches the $S(w) = S_0 \mathrm{sech}^2[(w - w_0)/\Delta w]$ fit to the experimental results, shown by the dotted curve (see Fig. 2), revealing excellent agreement.

Fig. 3 shows the corresponding pulse in the time domain. A Gaussian fit to the numerical data is once again quite poor, whereas a hyperbolic secant fit is found to agree well. The model predicts 1.57-ps hyperbolic secant pulses, which is consistent with the experimental measurements of Section II. Fig. 4 shows a simulated mode-locked pulse building up from noise (using a 1 photon/mode strength, complex, Gaussian-distributed, noise

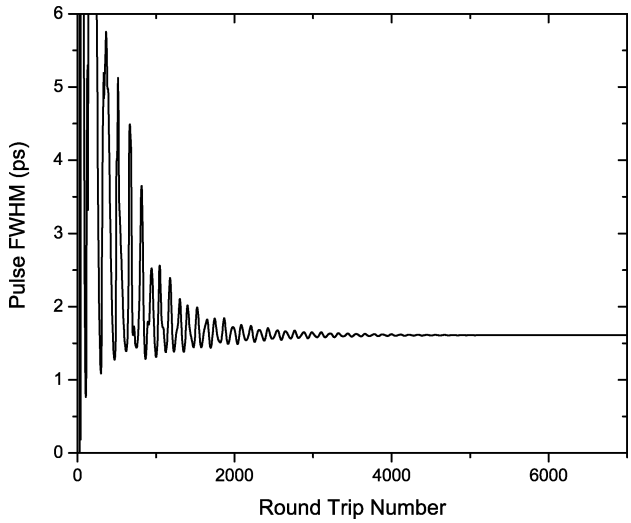

Fig. 5. Pulse temporal FWHM as a function of round-trip showing the numerical model converges to a steady state solution only after 5000 round-trips.

seed) over the first 2500 round-trips, while Fig. 5 shows the convergence of the pulsewidth to its steady state value. The large number of round-trips necessary before the mode-locked pulse converges is expected since the nonlinear and dispersive effects are weak over a single round-trip. As a consequence, many round-trips are required before the effects of nonlinearity and dispersion balance. Finally, the FWHM as a function of cavity location (after the model converged) varied by $<2\%$ revealing

that the pulse does not experience any large changes in width during a single round-trip.

IV. Stability

In the absence of dispersion and nonlinearity, an FM mode-locked laser will form pulses at either extreme [$\omega_m t+\phi = 0$ or π in (4)] of the modulation cycle. This behavior has been experimentally observed in lasers where the mode-locked pulse train shifts between these two temporal locations in a random fashion [13]. In their pioneering work [5], Kuizenga and Siegman noted that the degeneracy between these two states is broken when the modulation frequency is detuned from the laser's longitudinal mode spacing. This enables the gain medium to exhibit a dispersive effect. However they were unable to suppress this switching experimentally [13]. Later, Tamura and Nakazawa showed that the switching between the two states is suppressed in lasers with "large" intracavity dispersion, resulting in stable laser operation [14]. Depending on the sign of the cavity dispersion, the pulse at one of the two extremum will be spectrally broadened with respect to the other. The broader spectrum will experience more attenuation due to spectral filtering and the laser will operate in the other state to minimize loss [12], [14]. For example, mode-locked pulses pass through the modulator acquiring a positive chirp ($\omega_m t+\phi = 0$) in an anomalously dispersive cavity, while the modulator-induced chirp will be negative ($\omega_m t + \phi = \pi$) in a normally dispersive cavity [12], [14].

In this section we verify that our numerical model agrees with the findings of Tamura and Nakazawa [12], [14] by subjecting a mode-locked pulse to an abrupt phase jump in the modulator's driving electronics. This allows us to investigate the pulse switching mechanism in action, as well as the dynamical switching behavior. Using this approach we are able to identify two completely different pulse switching mechanisms.

To verify the numerical model predicts both stable and unstable temporal operating locations, the modulator's phase is abruptly changed after a mode-locked pulse is first formed. The theory, mentioned above, predicts that stable mode-locked pulses only form under the positive cycle of the FM modulator (in our anomalously dispersive cavity) and so the pulse is expected to temporally shift. In order to keep the pulses located within the central region of our simulation window, all the simulations in this section use $\phi = \pi/2$ [see (4)] which locates the extremum of the modulator at ± 24.25 ps. Fig. 6 shows the effect of a half-cycle clock phase shift (48.5 ps at 10.3 GHz or $\phi \rightarrow \phi + \pi$) on a mode-locked pulse. When the clock phase is shifted, at the 2000th round-trip, the pulse temporally broadens and eventually its power is redistributed amongst the two nearest stable modulator extremum. Although the pulse switches as expected, it only does so after first switching to what appears to be an unstable state, as shown by the constant pulse shape in Fig. 6 between round-trips 2500–6000.

To examine the switching mechanism in more detail, the temporal and spectral FWHM of the pulse were plotted as functions of round-trip and are shown in Fig. 7. After shifting the modulator's phase by π, the pulse experiences a short period of spectral compression whereas the pulse temporally broadens immediately; both are followed by a constant period

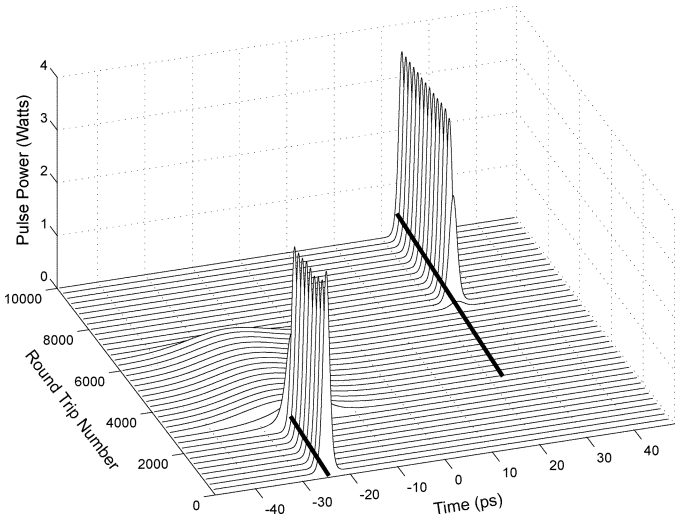

Fig. 6. Demonstration of pulse switching. The phase of the FM modulator was changed by π at the 2000th round-trip, shifting the location of the stable operating points, which have been identified by the solid lines to provide a convenient visual reference.

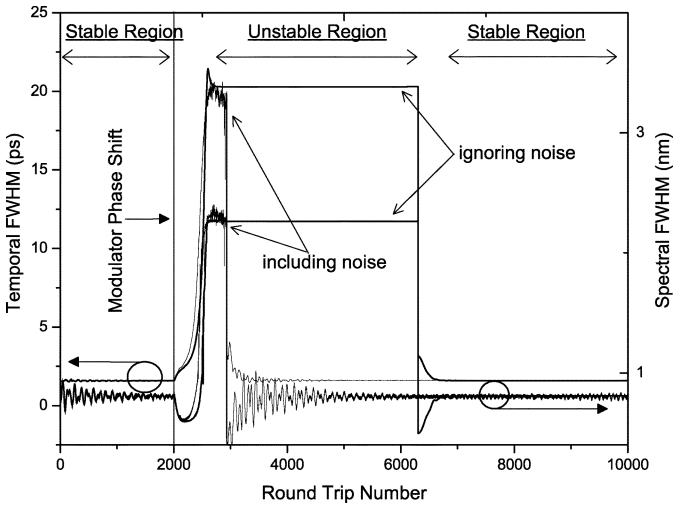

Fig. 7. Temporal and spectral FWHM as a function of round-trip, corresponding to the data plotted in Fig. 6. The location where the modulator's phase was shifted is identified as well as the stable and unstable operating regimes for case where noise was ignored. The same data is also plotted when noise was included in the numerical simulations and is labeled "including noise."

of broader bandwidth. To verify that this behavior is not related to a numerical anomaly, a noise term was added to (1) and the simulations were repeated. These results, labeled "including noise" in Fig. 7, reveal that even in the presence of noise there is a region after 2500 round-trips where the pulse spectrum and width stabilize. To explain this switching behavior, we note that the reduced spectral width found in the first transition region, between 2000 and 2500 round-trips, ensures that the effect of spectral filtering on the temporally broadening pulse is weaker than its effect on either the original pulse or the (newly shifted) stable pulse. This enables the pulse to continue broadening unabated. Since the pulse passes through the modulator extremum associated with an unstable state, it starts acquiring an unbalanced modulator-induced chirp. This chirp results in a drastic increase in the pulse spectrum

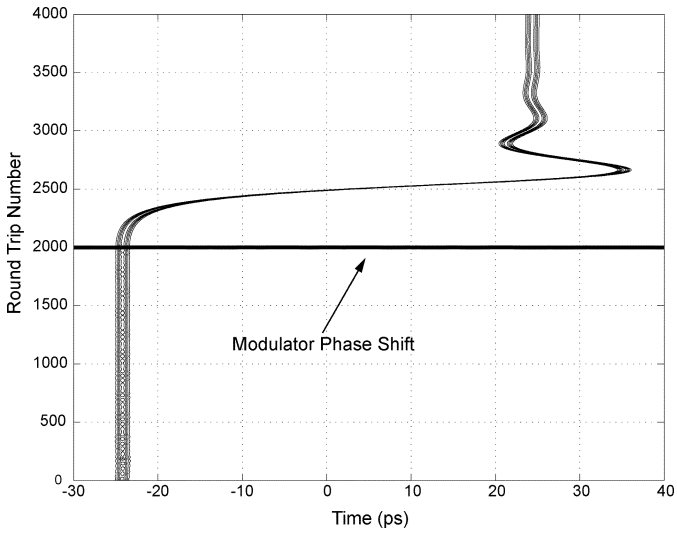

Fig. 8. Effect of TOD on pulse switching when the cavity's $\mathrm{TOD} > 0$. The pulse remains intact while temporally shifting to sync up with the (new) stable cycle of the modulator where it is once again stable.

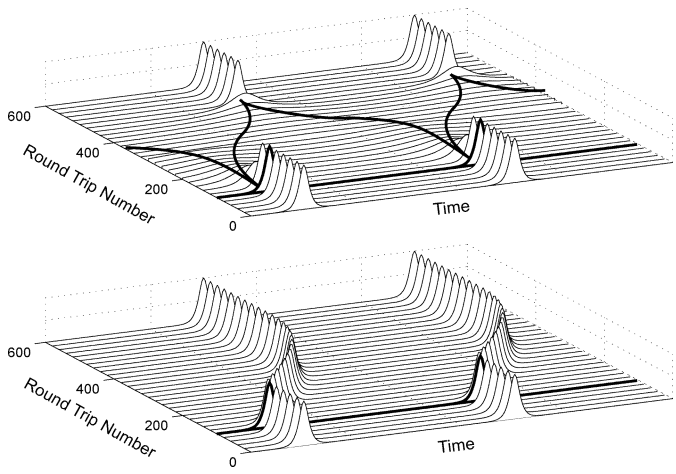

Fig. 9. Depiction of the energy transfer between modulation cycle locations when the driving frequency is abruptly changed by a half-clock cycle for the case where (a) SPM effects are weak and (b) SPM effects are important and $\mathrm{TOD} > 0$. The darkened trace in both plots, at the 100th round-trip, represents the location where the modulator's phase is shifted. The solid lines in (a) show how the energy from each pulse is redistributed.

around 2500 round-trips. Instead of this broadening continuing until the pulse switches states, the pulse becomes trapped in a local (globally unstable) potential due to an equalization between second-order dispersion, modulator-induced chirp, nonlinearity, and spectral filtering. The pulse remains in this unstable state, without changing shape, until it is destabilized by the formation of a stable pulse. The stable pulse has less bandwidth (0.8 nm compared to 2.26 nm see Fig. 7) than its unstable counterpart. As a consequence of spectral filtering, the stable pulse will experience less loss than the unstable pulse, thus providing the laser the incentive necessary to switch states. The only remaining question is how the laser actually switches between these two temporally displaced states. In our simulations we find that the stable pulses are seeded by the wings of the unstable pulse and by noise. As a consequence, when the noise was ignored many round-trips were required to reach a new equilibrium, whereas faster switching was observed in the presence of noise, since it provided a stronger seed (see Fig. 7).

It was previously found that the inclusion of SPM, whose sign is always positive, can prohibit mode-locking in the normal dispersion regime. This occurs because the modulator's pulse forming effect must overcome the pulse broadening effects of dispersion, nonlinearity, and spectral filtering in the normal dispersion regime for mode-locking to be possible. Although our laser operates in the anomalous dispersion regime, we can still investigate the role nonlinear effects play on the pulse switching by artificially doubling the saturation power while holding all other parameters constant. Fig. 8, which plots contours of constant intensity, examines this increased energy scenario using the same phase shift as before. This figure reveals a different switching mechanism where the pulse remains intact, shifting to the right side of the temporal window and settling down after about 2000 round-trips, but only after following a zig-zag path indicative of relaxation oscillations.

The pulse shift to the right side of the window in Fig. 8 is not incidental; it is governed by the sign of the cavity's net TOD. When the signs of the TOD for both fibers and the grating pair are flipped, the pulse moves to the left side of the temporal window while exhibiting identical dynamic features. These results, which constitute a temporal analog of a mirror image, can be understood by noting that the group velocity of a pulse is affected by finite values of TOD.

Although TOD was included in the model used to generate Fig. 6, the effect of SPM on the pulse was not strong enough to keep it intact when the modulator's phase was shifted; instead the pulse broadened while remaining centered on $\mathrm{t} = 0$. Fig. 9 summarizes our results using a cartoon (not a simulation) to focus on the effects of an abrupt phase change on two pulses in a harmonically mode-locked pulse train. Fig. 9(a) diagrammatically shows the effect of this switching mechanism on pulse energy when the switching is governed by the growth of a new pulse from the wings of the initial pulse and/or from noise. Fig. 9(b) examines the behavior found with increased power and positive TOD; the pulses shift in the opposite direction when TOD is negative. With their increased peak powers, the pulses seen in Figs. 8 and 9(b) can be viewed as "solitons," which are able to maintain their shape through the interplay between second-order dispersion and SPM, despite the perturbation from the FM modulator. They avoid dispersing long enough to experience the temporal kick of TOD, which sends these pulses to the stable operating points. In the absence of SPM, the pulses immediately broaden, as depicted in Fig. 9(a), and the effects of TOD are weakened. Larger values of TOD will encourage even these pulses to remain intact by "pushing" them toward a new equilibrium with increasing strength. However, a single pulse's energy will still be distributed between the two nearest final pulses. In this case the energy splitting will become asymmetric (from the perspective of the seed pulse), favoring one operating point over the other depending on the sign of the TOD. It is also noted that arbitrarily increasing the TOD will eventually disrupt the modulator's ability to synchronize the pulses, thus disabling the mode-locking mechanism altogether.

When the modulator's phase was abruptly changed, it was found that the (shifted) stable operating states were reached

more quickly with an increase in either the modulation depth or the anomalous dispersion value. The stable operating states were also reached more quickly when a spectral filter was used or the gain bandwidth was otherwise decreased. However, the repetition rate becomes important since it governs the temporal separation between the stable and unstable states. At lower repetition rates, the pulses are more prone to decay since they must shift between modulator extremum temporally separated by larger amounts. We also note that the effect of TOD on the picosecond pulses simulated is weak, and so switching should occur more quickly for femtosecond pulses. The large phase jump, used in this section for demonstration purposes, is impractical in a mode-locked laser under normal operating conditions. However, the different switching mechanisms identified in this section will still occur for smaller phase jumps (due to electronic noise, thermal effects, etc.) although it becomes more difficult to differentiate between them.

V. Ginzberg–Landau Equation

Although passive optical fibers support solitons in the anomalous-dispersion regime, (1) does not have a standard soliton solution because of the presence of gain and loss. In addition to this, none of the parameters β_2, β_3, γ, α, or g are constants, rather they all vary over the cavity length. This situation is analogous to long-haul lightwave systems in which fibers of two or more types are used to form a periodic dispersion map [24]. In such systems new types of solitons, known as dispersion-managed solitons, exist in the form of chirped Gaussian pulses [25]. We can, however, rule this possibility out in our fiber laser because the nonlinear and dispersive effects are relatively weak, and because the pulsewidth barely changes during a single round-trip. This is in sharp contrast to dispersion-managed lightwave systems where pulse width changes considerably. Of course the presence of a hyperbolic secant spectrum also clearly indicates that a Gaussian solution is not appropriate.

Another class of solitons exists in optical systems in which pulses experience gain and loss as they propagate. Such solitons are known as autosolitons [22] or dissipative solitons [26]. Since simulations show the pulsewidth does not change much during a single round-trip, and our output spectrum has a hyperbolic secant profile, the pulses emitted by our laser are more consistent with autosolitons than with dispersion-managed solitons. Recent investigations into fiber lasers mode-locked with multiple pulses also support this conclusion through the study of pulse interactions [27], [28]. To justify this claim, we average all the parameters used in Section III over one round-trip and write the resulting equation in the form [22], [23]

$$\frac{\partial A}{\partial z}+\frac{i}{2}\left(\bar{\beta}_2+i\bar{g}T_2^2\right)\frac{\partial^2 A}{\partial t^2}-\frac{1}{6}\bar{\beta}_3\frac{\partial^3 A}{\partial t^3} = i\bar{\gamma}\left|A\right|^2 A+\frac{1}{2}\left(\bar{g}-\bar{\alpha}\right)A+\frac{i2\Delta}{L}\cos(\omega_m t+\phi)A \quad (5)$$

where the overbar denotes the averaged value of the corresponding parameter, i.e., $\bar{\beta}_2 = 1/L\int_0^L \beta_2(z)dz$ and so on. Finite gain bandwidth is again assumed to have a parabolic filtering effect with a spectral width given by $T_2 = 2/\Delta w_g = 47$ fs/rad. The averaged saturated gain is given by $\bar{g} = \bar{g_0}\left(1+\bar{P}_{\rm ave}/P_{\rm sat}\right)^{-1}$ where $\bar{P}_{\rm ave}$, the average intracavity power, is now a constant and, therefore, location independent.

The strength of the modulation term in (5) was computationally found to have only a weak effect on the final pulse shape and width, so by assuming that we already have a pulse the modulator's effect can be neglected in this equation. We also note that actively mode-locked lasers are usually dominated by second-order dispersion and rarely produce pulses in the femtosecond regime. One can use this as an argument to ignore the effects of TOD. Under such conditions, this equation reduces to the well known Ginzburg–Landau equation which has the shape-preserving autosoliton [22] solution

$$A(z,t)=N_s\mathrm{sech}\left(\frac{t}{\tau}\right)^{1+iq}\exp(ikz) \quad (6)$$

where

$$\tau^2=\frac{\bar{g}T_2^2+\bar{\beta}_2 q}{\bar{g}-\bar{\alpha}}, \quad (7)$$

$$N_s^2=\frac{1}{2\gamma\tau^2}\left[\left(q^2-2\right)\bar{\beta}_2+3\bar{g}T_2^2 q\right] \quad (8)$$

$$k=-\frac{1}{2\tau^2}\left[\left(1-q^2\right)\bar{\beta}_2-2\bar{g}T_2^2 q\right] \quad (9)$$

$$q=\frac{3\bar{\beta}_2}{2\bar{g}T_2^2}\pm\sqrt{\left(\frac{3\bar{\beta}_2}{2\bar{g}T_2^2}\right)^2+2}\,. \quad (10)$$

Equations (7)–(10) require the value of $\bar{g}$ which depends on $\bar{P}_{\rm ave}$, itself a function of τ [(7)] and N_s [(8)], and so we have an underdetermined system. In order to circumvent this problem without introducing error, the value of $\bar{g}$ was obtained by numerically solving (5). The resulting value was then used in (7)–(10) to determine the parameters for the shape of the temporal field.

This analytic solution should be compared with the numerical results obtained in Section III before one can claim that our mode-locked laser emits autosolitons. To facilitate such a comparison, we note that the chirp parameter, q, may be computationally determined for an autosoliton via

$$q=\frac{i}{E}\int_{-\infty}^{\infty} t\left[A^*\frac{\partial A}{\partial t}-A\frac{\partial A^*}{\partial t}\right]. \quad (11)$$

Using the values $\bar{\beta}_2 = -1.435\,45\times10^4$ fs^2/m, $\bar{\beta}_3 = 29.7273\times10^4$ fs^3/m, $\bar{\gamma} = 0.012$ W^{-1}/m, $\bar{\alpha} = 0.782\,277\,1$ m^{-1}, and $\bar{g} = 0.782\,752\,5$ m^{-1}, the autosoliton approach predicts $\tau = 1.1058$ ps, and $q = 0.0802$. To compare these values with the numerical model we extract the field at "output 2" [See Fig. 1(b)] where it is expected to have the minimal (map-induced) chirp and, therefore, be consistent with an autosoliton. The numerical model predicts pulses with $\tau = 0.8912$ ps and $q = 0.0117$, yielding less than ideal agreement with the autosoliton theory.

Although we have been advocating the idea that the mode-locked pulses are autosolitons, based on the governing equation and recent work [27], [28], the merits of treating the pulses as fundamental solitons may also be investigated. By substituting $(A^{\pm}(z,t) = A_0\mathrm{sech}(t/\tau)e^{\pm ikz})$ into (3), using both $P_{\rm ave} = P^+_{\rm ave}(z)+P^-_{\rm ave}(z) = 2P^+_{\rm ave}$ (since the power is constant in the

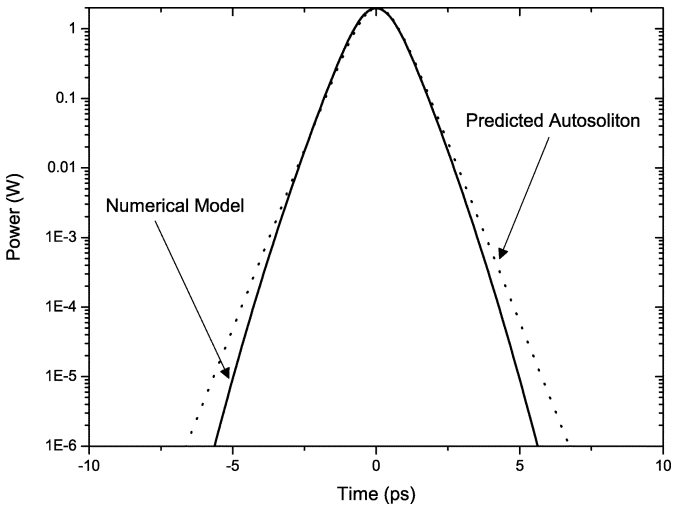

Fig. 10. Temporal profile of the numerically simulated pulse (solid) and the predicted autosoliton (dotted).

average model) and the fundamental soliton condition ($L_D = L_{NL}$), we arrive at the pulsewidth predicted by conventional soliton theory (assuming the cavity dispersion is anomalous)

$$\tau = \frac{4F_{\rm rep}|\bar{\beta}_2|}{\bar{\gamma}P_{\rm ave}}. \tag{12}$$

Using our numerically obtained average power, $P_{\rm ave} = 35.928$ mW, and assuming a standard soliton we find that $\tau = 1.372$ ps and of course $q = 0.0000$. Although neither prediction is accurate, the autosoliton theory is 30% closer to the numerically obtained width than the soliton theory. This indicates that there is certainly a distinction to be made between these two types of solitons in fiber lasers.

Further investigation shows that the poor agreement between autosoliton theory and numerical modeling can be attributed to the high intracavity losses in our laser, which makes the use of the average model questionable. To model a laser with lower intracavity losses, the fraction of the power re-entering the fiber in the HR2 arm was increased from 4% to 60% and the gain was decreased to $g_0 = 1.2\ \mathrm{m}^{-1}$, in order to maintain the same power level. Using these parameters the full model gives a temporal pulsewidth of $\tau = 0.8578$ ps and a chirp parameter $q = 0.0027$, whereas the autosoliton theory predicts a pulsewidth of $\tau = 0.8412$ ps, and a pulse chirp parameter $q = 0.0172$. Fig. 10 compares the pulse shape obtained from the full model to the pulse predicted by autosoliton theory using these values. Although excellent agreement is obtained for the pulsewidth and temporal shape (as seen in Fig. 10), the chirp parameters are once again in poor agreement.

Our results suggest that the existence of a dispersion map is at the root of the poor agreement for the chirp parameter q; after all the dispersion map causes q to vary within the cavity. We verified this statement by eliminating the grating pair and adjusting the dispersion such that it is constant inside the laser in the numerical model of Section III. Under such conditions, the predictions of autosoliton theory agree with the numerical model within a few percent. Although perfect agreement is not expected due to the effects of TOD (which is primarily responsible for the deviation between pulse shapes seen in Fig. 10) and the mode-locker, which were both ignored in assuming the autosoliton pulse shape, we conclude that the mode-locked pulses emitted by our laser are essentially in the form of autosolitons. Despite the autosoliton solution, a laser will not form mode-locked pulses on its own; a mode-locking element is always required. However, the active fiber will always try to impose the autosoliton shape on any pulse circulating within the cavity. We point out that this reasoning was previously used by Haus and Silberberg in their investigation of AM mode-locking in the anomalous-dispersion regime with nonlinearity [6]. Therefore, if the effect of the mode-locking element on the field is weaker than this active fiber shaping mechanism, as is frequently the case in FM mode-locking, this shaping mechanism will dominate and we will essentially end up with autosolitons.

VI. Conclusion

In conclusion, this work examined a high-repetition-rate, harmonically, FM-mode-locked, ytterbium fiber laser experimentally, numerically, and analytically. Pulse stability was investigated and the role of TOD and the unstable modulator extremum on abrupt phase jumps in an FM mode-locked laser was investigated for what we believe to be the first time. The short cavity length and low peak powers allowed us to approximate the pulse dynamics with an average model given by a modified Ginzberg–Landau equation. The averaged equation was then analytically investigated assuming the laser is mode-locked with an autosoliton. The results of this analytic theory were compared to the numerical results and found to be in good agreement in a lower-loss laser cavity. Such a treatment of the laser also shows that the effect of the FM modulator on the field is much weaker than the active fiber and thus appears only as a small perturbation. This fact reveals that active-fiber based pulse shaping is the overriding pulse shaping mechanism in this laser.

Strictly speaking, this type of laser is expected to have a pulse consistent with an autosoliton, as opposed to a standard soliton. In fact any deviation from the autosoliton shape may be attributed to the fact that this laser does, in reality, have a dispersion map with finite TOD, an FM modulator, and discreet losses. Although the distinction between these two types of solitons is subtle for actively mode-locked lasers producing picosecond pulses, we believe that it should be more pronounced at higher modulation frequencies which are able to produce shorter pulses that will experience stronger spectral filtering, resulting in a larger gain/loss imbalance and, hence, an increased chirp.

References

[1] G. P. Agrawal, *Nonlinear Fiber Optics*, 3rd ed. San Diego, CA: Academic, 2001.

[2] L. E. Nelson, D. J. Jones, K. Tamura, H. A. Haus, and E. P. Ippen, "Ultrashort-pulse fiber ring lasers," *Appl. Phys. B*, vol. 65, pp. 277–294, 1997.

[3] M. Hofer, M. H. Ober, F. Haberl, and M. E. Fermann, "Characterization of ultrashort pulse formation in passively mode-locked fiber lasers," *IEEE J. Quantum Electron.*, vol. 28, no. 3, pp. 720–728, Mar. 1992.

[4] T. F. Carruthers and I. N. Duling III, "10-GHz, 1.3-ps erbium fiber laser employing soiton pulse shortening," *Opt. Lett.*, vol. 21, pp. 1927–1929, 2002.

[5] D. J. Kuizenga and A. E. Siegman, "FM and AM mode locking of the homogeneous laser–Part I: Theory," *IEEE J. Quantum Electron.*, vol. QE-6, no. 11, pp. 694–708, Nov. 1970.

[6] H. A. Haus and Y. Silberberg, "Laser mode locking with addition of nonliner index," *IEEE J. Quantum Electron.*, vol. QE-22, no. 2, pp. 325–331, Feb. 1986.
[7] J. D. Kafka, T. Baer, and D. W. Hall, "Mode-locked erbium-doped fiber laser with soliton pulse shaping," *Opt. Lett.*, vol. 15, pp. 1269–1271, 1989.
[8] F. X. Kärtner, D. Kopf, and U. Keller, "Solitary-pulse stabilization and shortening in actively mode-locked lasers," *J. Opt. Soc. Amer. B*, vol. 12, pp. 486–496, 1995.
[9] A. M. Dunlop, W. J. Firth, and E. M. Wright, "Pulse shapes and stability in Kerr and active mode-locking (KAML)," *Opt. Exp.*, vol. 2, pp. 204–211, 1998.
[10] J. G. Caputo, C. B. Clausen, M. P. Sørensen, and S. Bischoff, "Amplitude-modulated fiber-ring laser," *J. Opt. Soc. Amer. B*, vol. 17, pp. 705–712, 2000.
[11] W. Lu, L. Yan, and C. R. Menyuk, "Soliton stability conditions in actively mode-locked inhomogeneously broadened lasers," *J. Opt. Soc. Amer. B*, vol. 20, pp. 1473–1478, 2003.
[12] M. Nakazawa, E. Yoshida, and K. Tamura, "10 GHz, 2 ps regeneratively and harmonically FM mode-locked erbium fiber ring laser," *Electron. Lett.*, vol. 32, pp. 1285–1287, 1996.
[13] D. J. Kuizenga and A. E. Siegman, "FM and AM mode locking of the homogeneous laser–Part II: Experimental results in a Nd:YAG laser with internal FM modulation," *IEEE J. Quantum Electron.*, vol. QE-6, no. 11, pp. 709–715, Nov. 1970.
[14] K. Tamura and M. Nakazawa, "Pulse energy equalization in harmonically FM mode-locked lasers with slow gain," *Opt. Lett.*, vol. 21, pp. 1930–1932, 1996.
[15] M. W. Phillips, A. I. Ferguson, and D. C. Hanna, "Frequency-modulation mode locking of a Nd^{3+}-doped fiber laser," *Opt. Lett.*, vol. 14, pp. 219–221, 1989.
[16] M. Nakazawa and E. Yoshida, "A 40-GHz 850-fs regeneratively FM mode-locked polarization-maintaining erbium fiber ring laser," *IEEE Photon. Technol. Lett.*, vol. 12, no. 12, pp. 1613–1615, Dec. 2000.
[17] E. Yoshida, K. Tamura, and M. Nakazawa, "Intracavity dispersion effects of a regeneratively and harmonically FM mode-locked erbium-doped fiber laser," *IEICE Trans. Electron.*, vol. E81-C, pp. 189–194, 1998.
[18] N. G. Usechak, J. D. Zuegel, and G. P. Agrawal, "Tunable, high repetition-rate, harmonically mode-locked, ytterbium fiber laser," *Opt. Lett.*, vol. 29, pp. 1360–1362, 2004.
[19] F. Ö. Ilday, J. Buckley, L. Kuznetsova, and F. W. Wise, "Generation of 36-fs pulses from a ytterbium fiber laser," *Opt. Exp.*, vol. 11, pp. 3550–3554, 2003.
[20] W. H. Knox, "*In situ* measurement of complete intracavity dispersion in an operating Ti:sapphire femtosecond laser," *Opt. Lett.*, vol. 17, pp. 514–516, 1992.
[21] J. M. Roth, T. E. Murphy, and C. Xu, "Ultrasensitive and high-dynamic-range two-photon absorption in a GaAs photomultiplier tube," *Opt. Lett.*, vol. 27, pp. 2076–2078, 2002.
[22] G. P. Agrawal, *Applications of Nonlinear Fiber Optics*. New York: Academic, 2001.
[23] S. Wabnitz, "Suppression of soliton interactions by phase modulation," *Electron. Lett.*, vol. 19, pp. 1711–1713, 1993.
[24] R.-M. Mu, V. S. Grigoryan, and C. R. Menyuk, "Comparison of theory and experiment for dispersion-managed solitons in a recirculating fiber loop," *IEEE J. Sel. Top. Quantum Electron.*, vol. 6, no. 2, pp. 248–257, Mar.–Apr. 2000.
[25] N. J. Smith, F. M. Knox, N. J. Doran, K. J. Blow, and I. Benion, "Enhanced power solitons in optical fibers with periodic dispersion management," *Electron. Lett.*, vol. 32, pp. 54–55, 1996.
[26] N. N. Akhmediev, A. Ankiewicz, and J. M. Soto-Crespo, "Stable soliton pairs in optical transmission lines and fiber lasers," *J. Opt. Soc. Amer. B*, vol. 15, pp. 515–523, 1998.
[27] M. Olivier, V. Roy, and M. Piché, "Pulse collisions in the streched-pulse fiber laser," *Opt. Lett.*, vol. 29, pp. 1461–1463, 2004.
[28] P. Grelu and N. Akhmediev, "Group interactions of dissipative solitons in a laer cavity: The case of 2+1," *Opt. Exp.*, vol. 12, pp. 3184–3189, 2004.

Nicholas G. Usechak was born in Long Branch, NJ, in 1976. He received the B.S. degrees with high honors in both electrical engineering and engineering physics from Lehigh University, Bethlehem, PA, in 2000, and the M.S. degree in optical engineering from the Institute of Optics, University of Rochester, Rochester, NY, in 2003, where he is currently pursuing the Ph.D. degree.

At Lehigh University, he was a Presidential Scholar during the academic year 1999–2000, and at the University of Rochester, he is currently a Frank J. Horton Fellow. His research interests include nonlinear fiber optics, fiber lasers, and ultrafast optics.

Mr. Usechak is a Student Member of the OSA, Tau Beta Pi, and Sigma Xi.

Govind P. Agrawal (M'83–SM'86–F'96) received the B.S. degree from the University of Lucknow, India, in 1969, and the M.S. and Ph.D. degrees from the Indian Institute of Technology, New Delhi, in 1971 and 1974, respectively.

After holding positions at the Ecole Polytechnique, Palaiseau, France, the City University of New York, New York, and the AT&T Bell Laboratories, Murray Hill, NJ, Dr. Agrawal joined the faculty of the Institute of Optics at the University of Rochester, Rochester, NY in 1989, where he is currently a Professor of Optics. His research interests focus on optical communications, nonlinear optics, and laser physics. He is an author or coauthor of more than 300 research papers, several book chapters and review articles, and five books entitled *Semiconductor Lasers* (Norwell, MA: Kluwer Academic, 2nd ed., 1993), *Fiber-Optic Communication Systems* (New York: Wiley, 3rd ed., 2002), *Nonlinear Fiber Optics* (New York: Academic, 3rd ed., 2001), *Applications of Nonlinear Fiber Optics* (New York: Academic, 2001), and *Optical Solitons: From Fibers to Photonic Crystals* (New York: Academic, 2003). He has also edited two books: *Contemporary Nonlinear Optics* (New York: Academic, 1992) and *Semiconductor Lasers: Past, Present and Future* (New York: AIP, 1995).

Dr. Agrawal is a Fellow of the Optical Society of America (OSA). He has participated multiple times in organizing technical conferences sponsored by OSA and IEEE. He was the Program Co-Chair in 1999 and the General Co-Chair in 2001 for the Quantum Electronics and Laser Science Conference. He was a Member of the Program Committee in 2004 for the Conference on Lasers and Electrooptics (CLEO).

Jonathan D. Zuegel received the B.S. and M.Eng. degrees in electrical engineering from Cornell University, Ithaca, NY, in 1983 and 1984, respectively. After servicing the in the U.S. Navy, he returned to graduate school at the University of Rochester, Rochester, NY, where he received the Ph.D. degree in optics from The Institute of Optics in 1996.

He is a Scientist and Group Leader of the Laser Technology Development Group at the Laboratory for Laser Energetics (LLE) located at the University of Rochester. Dr. Zuegel joined LLE in 1996 where he has contributed to the development of numerous solid-state laser and electro-optic systems for the OMEGA laser system.